NEOPLASIA
www.neoplasia.com

Volume 11 Number 4 April 2009 pp. 355–364 355

Discovery of Fully Human Anti-MET Monoclonal Antibodies with Antitumor Activity against Colon Cancer Tumor Models *In Vivo*[1]

Edward Htun van der Horst*, Lawrence Chinn*, Min Wang*, Timothy Velilla*, Hoang Tran†, Yarrow Madrona†, Andrew Lam†, May Ji†, Timothy C. Hoey* and Aaron K. Sato†

*Department of Cancer Biology, OncoMed Pharmaceuticals Inc., 800 Chesapeake Dr., Redwood City, CA 94063, USA; †Department of Molecular Biology, OncoMed Pharmaceuticals Inc., 800 Chesapeake Dr., Redwood City, CA 94063, USA

Abstract

The receptor tyrosine kinase MET is a major component controlling the invasive growth program in embryonic development and in invasive malignancies. The discovery of therapeutic antibodies against MET has been difficult, and antibodies that compete with hepatocyte growth factor (HGF) act as agonists. By applying phage technology and cell-based panning strategies, we discovered two fully human antibodies against MET (R13 and R28), which synergistically inhibit HGF binding to MET and elicit antibody-dependent cellular cytotoxicity. Cell-based phosphorylation assays demonstrate that R13 and R28 abrogate HGF-induced activation of MET, AKT1, ERK1/2, and HGF-induced migration and proliferation. FACS experiments suggest that the inhibitory effect is mediated by "locking" MET receptor in a state with R13, which then increases avidity of R28 for the extracellular domain of MET, thus blocking HGF binding without activating the receptor. *In vivo* studies demonstrate that the combination of R13/28 significantly inhibited tumor growth in various colon tumor xenograft models. Inhibition of tumor growth was associated with induction of hypoxia. Global gene expression analysis shows that inhibition of HGF/MET pathway significantly upregulated the tumor suppressors KLF6, CEACAM1, and BMP2, the negative regulator of phosphatidylinositol-3-OH-kinase PIK3IP1, and significantly suppressed SCF and SERPINE2, both enhancers of proliferation and invasiveness. Moreover, in an experimental metastasis model, R13/28 increased survival by preventing the recurrence of otherwise lethal lung metastases. Taken together, these results underscore the utility of a dual-antibody approach for targeting MET and possibly other receptor tyrosine kinases. Our approach could be expanded to drug discovery efforts against other cell surface proteins.

Neoplasia (2009) 11, 355–364

Introduction

Colorectal cancer (CRC) is one of the most prevalent forms of cancer with new cases and 500,000 deaths annually [1]. It remains the third most common cancer in men and women in the United States [2]. In 30% to 40% of CRC patients, metastases are confined to the liver, and for one quarter to one third of patients who are able to undergo resection of liver metastases, the median survival after resection is between 24 and 40 months [3]. Thus, this high rate of liver metastases has transformed treatment and evaluation and needs to be aggressively addressed to improve cure rates.

Numerous studies have implicated aberrant function of the receptor tyrosine kinase MET in the progression and metastasis of human tumors including carcinoma of the pancreas, stomach, prostate, ovary, breast, hepatocarcinoma, gastrinoma, melanoma, osteosarcoma, and CRC [4]. The most frequent occurrence in human tumors is the increased

Abbreviations: CRC, colorectal cancer; HGF, hepatocyte growth factor

Address all correspondence to: Dr. Edward Htun van der Horst, Department of Cancer Biology, OncoMed Pharmaceuticals Inc., 800 Chesapeake Dr., Redwood City, CA 94063. E-mail: edward.vanderhorst@oncomed.com

[1]This article refers to supplementary materials, which are designated by Table W1 and Figures W1 to W4 and are available online at www.neoplasia.com.

Received 4 December 2008; Revised 8 January 2009; Accepted 9 January 2009

DOI 10.1593/neo.81536

expression of MET in the absence of autocrine HGF production [5]. Increased MET signaling in early stage CRC is a common occurrence, whereas elevated MET expression/amplification in advanced disease is linked to metastatic progression, which, consequently, makes it a viable target for a significant subset of advanced CRC [6,7]. MET, which is the receptor of hepatocyte growth factor (HGF), is known to be responsible for controlling the invasive growth program during embryogenesis and in malignant cancer cells [4,5]. MET specifically stimulates cell scattering, invasion, protection from apoptosis and angiogenesis and therefore has become a candidate for targeted therapeutic intervention [8]. Several pharmaceutical companies have successfully discovered and developed small molecule inhibitors of MET, which currently are being tested in clinical trials [8]. Although one therapeutic antibody against HGF has entered the clinic, the discovery of therapeutic antibodies against MET has been very difficult, and antibodies that compete with HGF typically act as agonists by dimerizing the receptor [9]. As a consequence, therapeutic antibodies (e.g., 5D5) were engineered to be monovalent to be developed for clinical settings [10].

Whereas screening antibodies for HGF inhibition typically results in antibodies with agonist activity, in the present study, we tested an alternative approach. We hypothesized that, in cancer cell lines with a very high level of MET expression, the receptor exists, at least partially, in a ligand-independent active conformation. Therefore, we used a cell-based panning strategy against cancer cell lines with a genomic amplification of the MET locus. We identified two antibodies that synergistically inhibit MET signaling *in vitro* and *in vivo* and display therapeutic efficacy in a variety of tumor models. Our approach could be expanded to drug discovery efforts against other cell surface proteins.

Materials and Methods

General Materials

HuCAL GOLD library was from Morphosys (Martinsried, Germany) [11]. Recombinant human HGF was purchased from Peprotech (Rockyhill, NJ). Recombinant human MET/Fc chimeric protein (extracellular domain of MET, rMET-ECD-FC) was purchased from R&D Systems (Minneapolis, MN), rMET-ECD-HIS was obtained by stably overexpressing MET-ECD-H in 293-F (Invitrogen, Carlsbad, CA) cells and purifying collected supernatants to homogeneity. Antibodies raised against the following proteins were used: MET polyclonal rabbit antibody (prAb) C-12 (Santa Cruz Biotechnology, Santa Cruz, CA), phospho-MET (monoclonal rabbit antibody (mrAb) 3D7), phospho-AKT (mrAb 193H12), phospho-MAPK (mrAb 197G2) were from Cell Signaling (Danvers, MA), and SHC (prAb) and phosphotyrosine (monoclonal mouse antibody (mmAb 4G10)) were from UBI (Billerica, MA). Phosphospecific and total protein ELISA kits for MET-(Y1230/Y1234/Y1235), MET-(Y1349), AKT1-(S473), and ERK1/2 were purchased from Invitrogen. As a control antibody, we used a murine IgG1 antibody (1B711) that recognizes a hapten, trinitrophenol. The cell lines A549, SNU-5, and H441 were obtained from ATCC (Manassas, VA), human umbilical vein endothelial cells (HUVECs) were from Cambrex (Charles City, IA) and cultured according to the suppliers' protocols. Collagen I–coated culture dishes and Matrigel were from BD Biosciences (Bedford, MA). DELFIA-EuTDA cytotoxicity reagents were from Perkin-Elmer (Waltham, MA). TaqMan assays for HGF, MET, GUS-B, High-Capacity cDNA Archive Kit and TaqMan PCR master mix were from Applied Biosystems (Foster City, CA).

HGF/MET Blocking Assay

Maxi-sorp 384-well microtiter plates (Nunc, Rochester, NY) were coated with recombinant human HGF (1 μg/ml × 25 μl; R&D Systems) at room temperature for 2 hours at 30°C. After washing the wells once with PBS–0.2% Tween-20 they were blocked with 5% PBS/milk for 1 hour. Anti-MET antibodies (FAb) were preincubated with MET-FC (25 ng per well) at room temperature for 1 hour. The FAb/MET-FC mixtures was then added to the HGF-coated wells and allowed to incubate for 1 hour at room temperature on a rocker and washed three times with PBS–0.2% Tween-20. The secondary antibody (goat antihuman FC, HRP-conjugated) was added at 1:5000 dilution and allowed to incubate for 1 hour at room temperature. Washing was done as above. Fifty microliters of substrate was added per well until a yellow color developed. The reaction was stopped with 50 μl of 1 M H_2SO_4, and the absorbance at 450 nm was determined with a standard plate reader.

Antibody-Dependent Cellular Cytotoxicity Assay

Blood was collected from normal volunteers and mixed with 33% (v/v) volume of PBS. The mixture was layered onto a Ficoll gradient and centrifuged at 400*g* for 40 minutes. Peripheral blood mononuclear cells were collected at the interface and washed thrice in PBS. GTL-16 cells were europium-labeled according to the manufacturer's protocol and plated at a density of 10,000 cells per well in 50 μl in a 96-well U-bottomed plate and were incubated with the indicated anti-MET antibodies (50 μl) at 37°C for 30 minutes. Peripheral blood mononuclear cells were added to triplicate wells in a volume of 100 μl at an effector/tumor cell ratio of 100:1 and were incubated at 37°C for 4 hours. Target maximum fluorescence was determined by lysing the cells with 10 μl of lysis buffer, whereas target spontaneous fluorescence was determined in the absence of antibody and effector cells. The percentage of specific cell lysis mediated by the antibodies was calculated as the percentage of cell lysis in the antibody-treated group: (experimental EM 615 nm – target spontaneous) / (target maximum – target spontaneous) × 100.

Western Immunoblot Analysis (HUVEC) and ELISAs (A549)

Western blot analysis was done as described previously [12]. Briefly, HUVEC or A549 cells were plated onto culture plates and serum-starved for 24 hours. Cells either were left untreated or were pretreated with the indicated IgGs (30 μg/ml) for 1 hour after stimulation with 20 ng/ml recombinant human HGF for 15 minutes at 37°C. After HGF stimulation, the cells were lysed; lysates were cleared before protein concentrations were determined.

Phosphospecific and total protein ELISAs were carried out according to the manufacturers' protocol. Phosphospecific values were normalized by total protein content of the gene of interest.

FACS Experiment with R13 and R28

GTL-16 cells were nonenzymatically detached from cell culture plates, washed, and blocked with PBS/2% fetal calf serum for 30 minutes before incubating with the antibodies. One hundred micrograms of R13 and of R28 were chemically conjugated with fluorochrome AF-647 following the supplier's protocol (Invitrogen). Cells were then incubated with unlabeled and/or labeled R13/R28 at the indicated concentrations for 30 minutes at room temperature. After extensive washing, cells were resuspendend in PBS/2% fetal calf serum and analyzed by FACS.

Proliferation and Migration Assays

Human umbilical vein endothelial cells were plated at 8×10^4 cells/ml (proliferation assay) or 2.5×10^5 cells per well (migration assay) onto Collagen I–coated 96- or 24-well culture plates in complete media (serum and growth factors; EGM-2), incubated for 24 hours, and subsequently serum-starved for 24 hours in EBM-2 supplemented with 0.5% fetal bovine serum. For HGF-induced studies, HUVECs were preincubated with R13/28 (30 μg/ml) or SU11274 (1 μM) for 1 hour before adding HGF (50 ng/ml). Cells were incubated for 7 days, and cell number was quantified using Cell-Titer-Glo Reagent (Promega, Madison, WI) according to the manufacturer's protocol. For migration assays, a single scrape was made in the confluent monolayer in each well as described previously [13].

Assaying Hypoxia

Staining for hypoxic regions was performed as reported previously [14]. Briefly, to measure hypoxia, pimonidazole hydrochloride (HypoxyProbe; NPI, Burlington, MA), which forms long-lived protein adducts at partial pressure of oxygen less than approximately 10 mm Hg, was injected intraperitoneally at 60 mg/kg into NOD/SCID or $nu^{-/-}$ mice 1 hour before sacrifice. Tumors were then processed for histologic analysis, and tumor sections (5 μm thick) were stained using antipimonidazole antibody. Photographs were taken using a BX51 microscope (Olympus, Center Valley, PA).

Xenograft Transplantation and Experimental Metastasis Experiments

OMP-C12, 27, and 28 are colon tumor xenograft lines used in this study, and they were established at OncoMed Pharmaceuticals by adhering to procedures described previously [15]. Immunocompromised male NOD/SCID mice were used for the establishment of OMP-C12, 27 and 28 tumor xenografts and female $nu^{-/-}$ (Swiss CD-1) mice were used for the GTL-16 tumor and experimental metastasis model (Harlan, Indianapolis, IN). Mice were subcutaneously injected on the right flank with 50,000 (for OMP-C12, 27, and 28) or 1×10^7 viable cells (GTL-16), respectively. Once the tumor has reached a size between 65 and 200 mm^3, mice were randomized.

Experimental metastasis assays were performed as described previously [16] with the exception that GTL-16-*luc* were used, and tumor burden in mice was visualized by noninvasive imaging with an IVIS200 instrument (Caliper, Mountain View, CA), as previously published [17]. Antibodies were administered weekly or as indicated, and tumors were measured twice weekly. Tumor volume was calculated as described [15]. All the experiments were performed on groups of at least 10 animals per experimental point. Animal experiments were performed in accordance with protocols approved by the OncoMed Pharmaceuticals Institutional Review Board – Animal Care and Use Committee.

Global Gene Expression Analysis

Global gene expression profiling analysis was performed on Affymetrix HG-U133 plus 2.0 microarray (Affymetrix, Santa Clara, CA). Three independent RNA samples of C27 xenograft whole tumors from the control and treatment groups were isolated and hybridized to the microarrays according to the manufacturer's instructions. Scanned array background adjustment and signal intensity normalization were performed with Gene Chip–Robust Multiarray Averaging algorithm in the open-source bioconductor software (www.bioconductor.org). Genes differentially expressed ($P < .05$ and fold change >2.0) between the two groups were identified with Bayesian *t*-test [18].

Median Effect and Combination Index Analysis

Drug interactions were analyzed using CalcuSyn (Biosoft, Cambridge, United Kingdom). This software calculates the median effect dose, D_m (analogous to the IC_{50}), of the drug combinations using the median effect equation. Determination of synergy or antagonism was based on the multiple drug effect equation of Chou and Talalay [19] and was quantified by the combination index (CI).

Statistical Analysis

Data are expressed as the mean and mean ± SEM. Group means were compared using Student's two-tailed unpaired *t* test. Probability (*P*) values of <.05 were interpreted as significantly different. Statistical analyses were performed by using Microsoft Excel (Microsoft, Redmond, WA) and GraphPad Prism (GraphPad Software, Inc., La Jolla, CA).

Results and Discussion

Our hypothesis was that, to obtain functional inhibitory antibodies against MET, the conformation of MET has to be in its active and functional conformation. Overexpression of receptor tyrosine kinases leads to multimerization of a subfraction of receptors and their subsequent activation [20]. The difficulty lies in enriching for FAbs, which recognize the active MET conformation, block binding of HGF without activating the inactive receptors. Therefore, we set out to identify antagonistic anti-MET antibodies by using the HuCAL phage display library and performing cell-based panning strategies [21] (Figure 1). We chose GTL-16 [22] and SNU-5 cancer cell lines owing to their high endogenous expression level of functional MET and their sensitivity to MET inhibition [23]. Moreover, by using two distinct cell lines, one adherent (GTL-16) and one suspension cell line (SNU-5), enrichment of cell surface receptors other than MET would be minimized. To increase

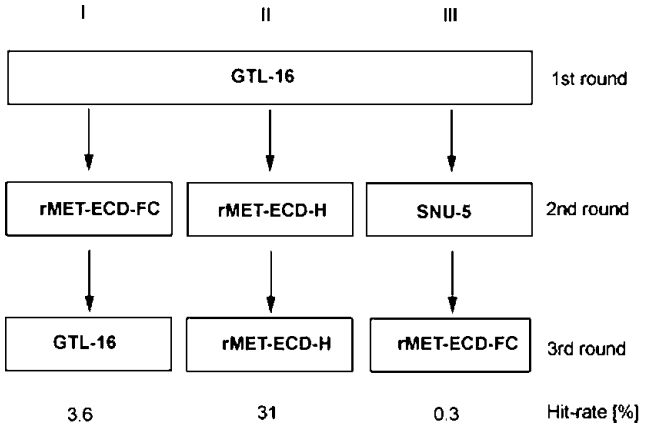

Figure 1. Panning strategy for inhibitory MET antibodies. Using the Morphosys HuCAL GOLD FAb library, functional anti-MET antibodies R13 and R28 were discovered using a series of novel selections against human cancer cell lines (GTL-16, SNU-5), which possess a MET amplicon ("active" MET), and recombinant Met extracellular domain (rMET-ECD-FC/H). Initially, all selections were initiated on GTL-16 cells (first round). The resulting output was split and selections continued with three different strategies: I) rMET-ECD-FC → GTL-16; II) rMET-ECD-H → rMET-ECD-H; III) SNU-5 → rMet-ECD-FC. The hit rate percentage (ELISA positive hits per 96-well plate) is indicated for each output. Please note that R28 was the only FAb from strategy III.

antibody specificity for the dimeric or monomeric form of the receptor, we also used recombinant extracellular domain of MET either as human Fc-fusion protein (rMET-ECD-FC) or as a 6× His-tagged protein (rMET-ECD-H), respectively. We started by panning the first round on live unfixed GTL-16 cells (Figure 1, *I–IV*). To enrich for leads, which would bind the dimeric or monomeric but presumably active state of MET, we panned then either on rMET-ECD-FC and GTL-16 (Figure 1, *I*) or panned two subsequent rounds on rMET-ECD-H (Figure 1, *II*), respectively. In strategy III, the second panning round was performed on SNU-5 and then further divided in two more rounds on rMET-ECD-FC (Figure 1, *III*). We discovered two specific anti-MET FAbs R13 (K_D[FAb] = 3.5 nM) and R28 (K_D[FAb] = 48 nM). Interestingly, R13 was obtained multiple times from strategies I and II, whereas R28 was discovered exclusively in output III but not from I or II. Epitope analysis revealed that only R13 binds to the SEMA domain of MET-ECD, whereas interestingly, R28 exclusively binds to the full-length molecule (Figure W1). Because it is known that the SEMA domain of MET-ECD is critical for HGF binding, our analysis suggests that R13 is a direct HGF competitor [24]. However, R28 also competes with HGF but does not bind to the critical SEMA domain of MET-ECD, indicating that R28 recognizes an epitope in its tertiary conformation. Therefore, binding of R28 to a tertiary structure of MET-ECD could lead to a conformational stabilization of the receptor, which prevents HGF binding to MET. Moreover, extensive efforts using selected subdomains of the rMET-ECD or starting the panning with recombinant protein instead of live cells always increased the hit rate but did not yield any FAbs with inhibitory properties (data not shown). This suggests that both the rMET-ECD and MET-ECD on cell lines exist in its native conformation, but the difference lies in its state of activity: "active" conformation on MET-dependent cells, whereas "inactive" conformation in its recombinant form.

We then performed a dose-response of R13 and R28 for their ability to block HGF binding to MET in a protein-protein interaction assay (Figure 2). Recombinant human HGF was passively immobilized to 384-well plates and used to capture rMET-ECD-FC preincubated with R13, R28, or a combination of both (Figure 2*A*). We observed that R13 and R28 with an IC_{50} of 8.88 nM and 30.3 nM, respectively, blocked ligand binding to MET (Figure 2*A*, *green and blue lines*).

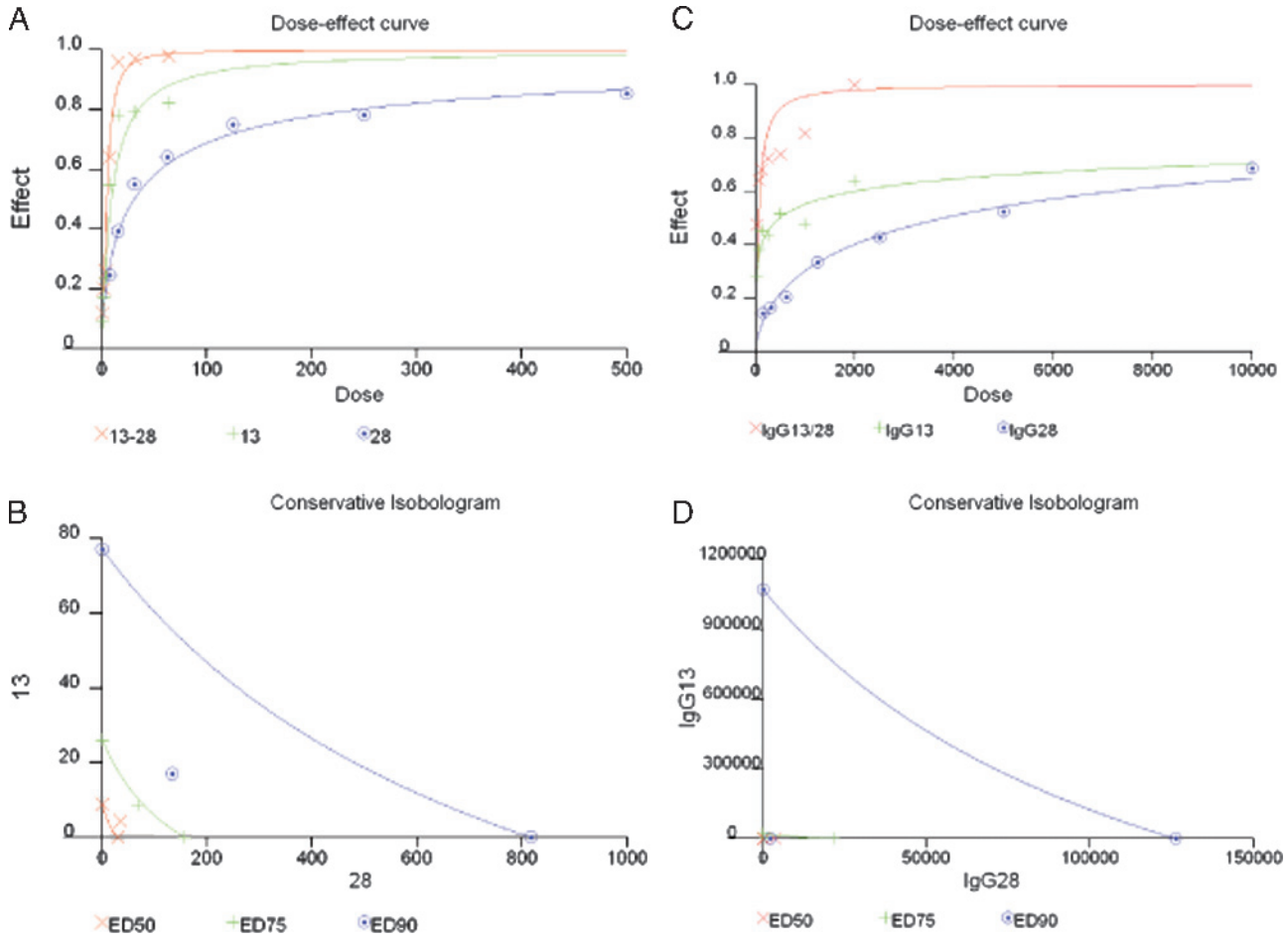

Figure 2. Combination of R13 and R28 synergistically inhibit HGF-binding to MET and induce ADCC. The effect (*y*-axis) of anti-MET antibodies R13 (green crosses), R28 (blue circles), and a combination of R13/28 (red ×'s) on blocking HGF binding to MET (A) and eliciting antibody-dependent cellular cytotoxicity in GTL-16 cancer cells (C) is shown for increasing doses of each antibody or antibody combination (*x*-axis; nM). The effect at each dose is marked with its corresponding symbol, and a dose-effect curve generated by curve fitting the data points for each antibody. A conservative isobologram demonstrates that the antibody combination R13/28 acts synergistically to block HGF binding to MET (B) and to induce ADCC (D). The ED_{50} (red ×), ED_{75} (green crosses), and ED_{90} (blue circles) are graphed. CI = 1 indicates an additive effect; <1, synergy; >1, antagonism. Results are shown for the mutually exclusive assumption of modes of activity of R13 and R28; however, applying the alternative assumption showed the same pattern of results. *ED* indicates effective dose.

Interestingly, the combination of R13 and R28 in a ratio of 1:5 more potently abrogated HGF binding to MET with an IC_{50} of 4.44 nM (Figure 2*A*, *red line*). Isobologram analysis revealed that the effect is synergistic, as the combination effectively induced either a 75% or a 90% effective dose (ED_{75} or ED_{90}) response that is well below the ED_{90} values induced by R13 or R28 alone (Figure 2*B*). Moreover, the CI value for ED_{90} and ED_{75} is 0.39 and 0.52, respectively, strongly suggesting that R13 and R28 act synergistically to inhibit ligand binding (Table W1).

It has been shown that therapeutic antibodies, such as anti–HER2 antibody (trastuzumab), not only abrogate signaling pathways but also induce antibody-dependent cellular cytotoxicity (ADCC), which significantly contribute to their antitumor activity in patients [25]. After reformatting R13 (K_D[IgG] = 0.9 nM) and R28 (K_D[IgG] = 1.9 nM) onto an IgG1 framework, we then tested them in ADCC assays with GTL-16 as target cells (Figure 2, *C* and *D*). R13 and R28 induced an ADCC with IC_{50} values of 479 nM and 3.77 μM, whereas the antibody combination strongly induced an ADCC with an IC_{50} of 58.9 nM (Figure 2*C*). Isobologram analysis and calculation of the CI values showed that the effect is strongly synergistic because the CI values at ED_{75} and ED_{90} were 0.04 and 0.02, respectively (Figure 2*D* and Table W1). These experiments demonstrate the synergistic properties of R13 and R28 in inhibiting HGF-MET binding and in inducing an ADCC response.

Because the HGF-MET axis plays a crucial role in angiogenesis and human umbilical vein endothelial cells (HUVECs) display high HGF response capability [26], we tested R13 and R28, both on an IgG1 framework, in cell-based HGF-induced phosphorylation wound healing and proliferation assays (Figure 3). To compare efficacy of R13 and R28, we also included the small molecule inhibitor of MET SU11274 as a positive control at 1 μM [27,28]. First, HUVECs were serum-starved for 24 hours, preincubated with the antibody combination R13/R28 or SU11274 for 1 hour at 37°C, and then stimulated with 20 ng/ml HGF for 15 minutes. We then analyzed the phosphorylation level of MET, of the downstream signaling molecules SHC and AKT1, and of ERK1. We observed that the HGF-induced tyrosine phosphorylation of MET, SHC, AKT1, and ERK1 was abrogated as efficiently by the antibody combination R13/28 as by SU11274 at 1 μM (Figure 3*A*, *upper panels*, *compare lane 2 to lanes 3 and 4*). Hepatocyte growth factor–induced proliferation assays were then performed to test the potential long-term inhibitory effect of R13/28 on HUVECs. We observed that antibody combination R13/28 inhibited HGF-induced proliferation by 69% (Figure 3*B*). Additionally, we performed wound healing assays with the MET-overexpressing cell line H441 and observed that wound healing was inhibited by 50% (Figure W2). We then used the HGF-sensitive lung cancer cell line A549 to test the inhibitory capability of the antibody combination R13/28 [29]. The extent of phosphorylation at the tyrosine residues Y1230/1234/1235 in the kinase domain and Y1349 in the cytoplasmic domain of MET and the phosphorylation of AKT1 at serine residue S-473 and ERK1/2 at threonine residues T185 and Y187 were quantified, and IC_{50} values were calculated (Table W1). The similarity of IC_{50} values in blocking the phosphorylation of Y1230/1234/1235 of MET and of AKT1 (MET-Y1230/1234/1235, IC_{50} = 49.5 nM *vs* AKT1-S-473, IC_{50} = 34.8 nM) indicates that inhibition of MET kinase activity directly results in the inhibition of AKT1. A similar correlation can be observed between IC_{50} values of the inhibition of Y1349 phosphorylation and ERK1/2 activation at T185 and Y187 (MET-Y1349, IC_{50} = 254 nM *vs* ERK1/2-T185/Y187, IC_{50} = 208 nM). This demonstrates that R13 and R28 abrogate MET signaling, resulting in the attenuation of crucial downstream signaling transducers thus leading to the inhibition of MET-mediated physiological responses.

Because the observed inhibitory effects are synergistic and the antibodies do not compete for the same epitope (Figure W1), we hypothesized that one antibody decreases the flexibility of MET, thereby enabling the other antibody to block the HGF binding site. We reasoned that one antibody would increase the binding of the other antibody to cells expressing MET in its active form. Therefore, we tested our hypothesis by titrating in one unlabeled antibody (R13 or R28) to the other AF647-conjugated antibody (R28 or R13) and then measuring the mean fluorescence intensity (MFI) on GTL-16 cells (Figure 3*C*). We observed that the ΔMFI values of AF647-conjugated R28 increased by increasing amounts of unlabeled R13. Because the K_D values remained unchanged (data not shown), this suggests that R13 increases the antigen accessibility of R28 for MET on GTL-16 cells, which leads to an increase in ΔMFI values. Conversely, unlabeled R28 did not increase R13-induced ΔMFI on GTL-16 cells. Now, we have to note that without crystal structure of either antibodies R13 and R28 with the full-length molecule MET, the detailed mechanism remains elusive, but structural studies are underway to clarify the proposed mechanism. However, taken together, this experiment indicates that antibody R13 facilitates the binding of R28 on GTL-16 cells, thereby potentiating the binding of R28 to MET-ECD and "locking" it into a nonfunctional receptor.

Consequently, we initiated proof-of-concept studies *in vivo* using GTL-16 cells and our colorectal tumor bank collection, which was established from patient primary tumors and passaged in NOD/SCID mice. First, we checked the RNA expression level of MET and HGF in our colon tumors (Figure W3). It has been reported that an increased expression of MET in the absence of autocrine produced HGF correlates with a metastatic phenotype and poor prognosis [5]. It has also been shown that MET protein expression is significantly higher in most primary adenocarcinomas of the colon than adjacent mucosa and that its expression level could serve as an early-stage invasion and regional metastasis marker [30,31]. In concordance with previous reports, we observed that colon tumors do not express the HGF transcript, which indicates that in CRC HGF is predominantly provided by the tumor-surrounding stroma (Figure W3). We then chose to test R13/28 in GTL-16, C12, C27, and C28 owing to their high MET expression levels and their intrinsic growth rates *in vivo*. Firstly, mice were subcutaneously injected with viable cells, and once the tumor reached a size between 65 and 200 mm^3, mice were randomized and subsequently treated with R13/28. We then tested the antibody combination R13/28 in a therapeutic *relevant* setting and observed that R13/28 was effective in inhibiting tumor growth in GTL-16, C12, C27, and C28 (Figure 4, *A–D*). Testing R13 and R28 individually showed no inhibitory effect on tumor growth (data not shown). Furthermore, histologic assessment showed extensive hypoxic areas in R13/28-treatment groups when compared with control C27 tumors (Figure 5*A*). Even more pronounced effects were observed when we repeated the experiment with GTL-16 cells: the combination R13/28 strongly inhibited GTL-16 tumor growth and increased hypoxic regions almost over the entire tumor surface area, especially in the center of the tumor (Figure W4). Healthy cells were only detectable at the rim of the GTL-16 tumors. Our data indicate that inhibition of MET signaling abrogated proangiogenic signals, which results in diminished tumor growth. This mechanism resembles the treatment of tumors with

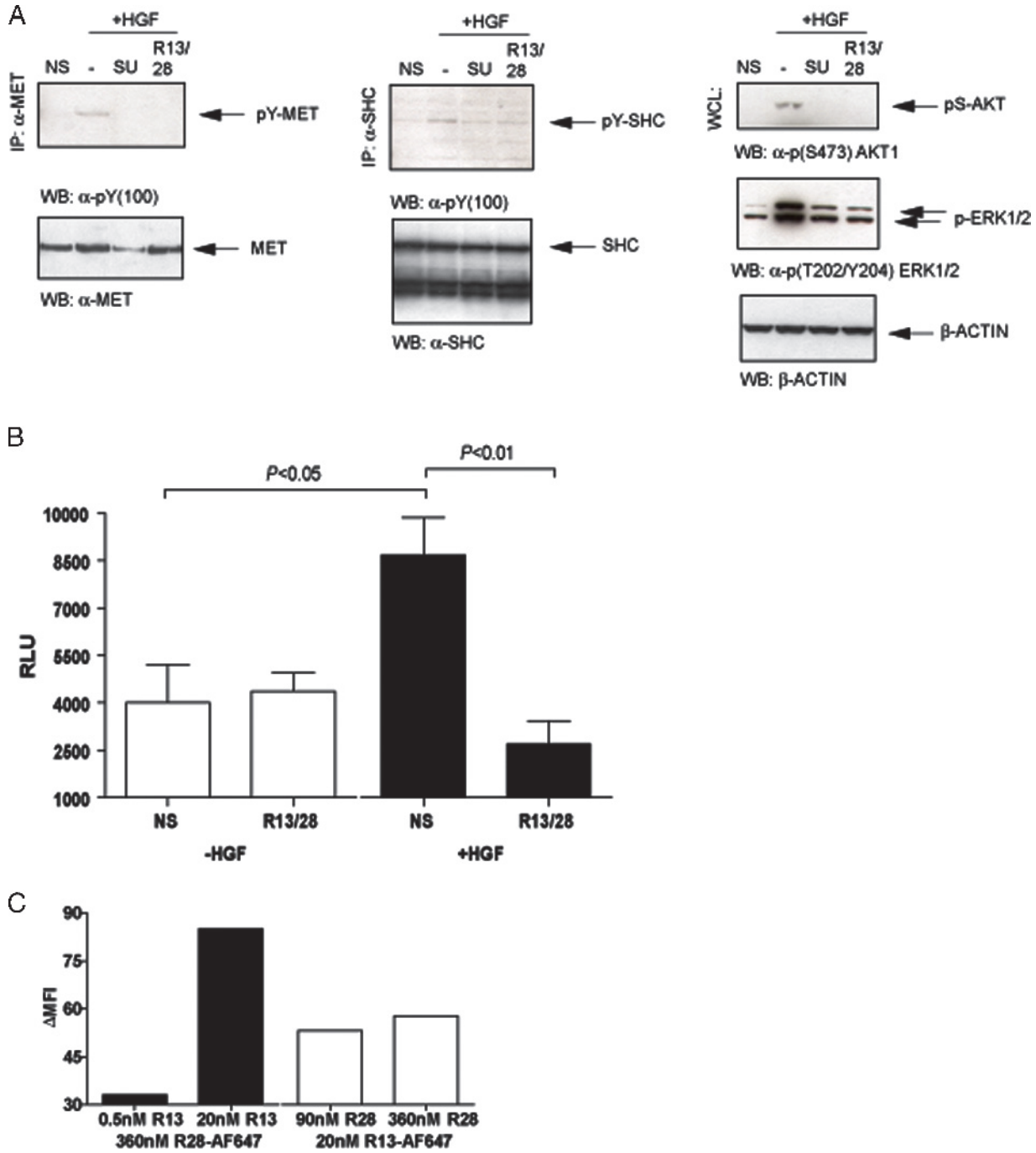

Figure 3. Combination of R13 and R28 inhibit HGF-mediated phosphorylation of MET, AKT, ERK1/2, and proliferation in HUVECs (A, B). Serum-starved HUVECs were either stimulated with HGF (20 ng/ml) for 15 minutes or pretreated with R13/28 (30 μg/ml) and SU11274 (SU, 1 μM) for 1 hour before HGF stimulation. Cell lysates were subjected to immunoprecipitation (IP) using antibodies against MET (α-MET; A, left panel) and SHC (α-SHC; A, middle panel). Phosphorylations of AKT1 and ERK1/2 were analyzed by Western blot analysis of whole cell lysates (WCLs) with anti–phospho-AKT antibody (α-p(S473)AKT1) (A, right top panel) or with phosphospecific anti-ERK1/2 antibody (α-p(T202/Y204)ERK1/2), respectively (A, right middle panel). Tyrosine phosphorylation was analyzed by Western blot analysis with monoclonal antiphosphotyrosine antibody (α-p(Y100)). Protein levels were checked by reblot analysis with antibodies against MET, SHC, or β-actin (A, lower panel). Serum-starved HUVECs were used in proliferation assays on Collagen I plates, pretreated with R13/28 (30 μg/ml) or SU11274 (SU, 1 μM), respectively, in the presence (black bars) or absence (white bars) of HGF (50 ng/ml) (B). Proliferation rate was increased 2.2-fold (Student's *t*-test, $P < .05$) in the presence of HGF. R13/28 suppressed HGF-induced proliferation to basal level (Student's *t*-test, $P < .01$) (B, compare black to white bars). Proliferation was measured after 7 days and was done twice in quadruplicates. Please note that R13/28–treated HUVECs are statistically equivalent to untreated cells. R13 enhances R28 avidity to MET receptor on GTL-16 cells (C). AF647-conjugated R28 (black bars) or R13 (white bars) was used as FACS reagent to detect MET receptor on GTL-16 cells. AF647-labeled antibodies (AF647-R28 or AF647-R13) were used at fixed concentrations (360 nM, AF647-R28; 20 nM, AF647-R13) and unlabeled R13 (0.5 nM, 20 nM) or R28 (90 nM, 360 nM) was titrated in. Note that 20 nM of R13 increased MFI values (ΔMFI) for AF647-R28 by 2.6-fold, whereas adding R28 to AF647-R13 did not show any effect. ΔMFI values were determined by subtracting background MFI. *NS* indicates not stimulated. Arrows indicate the detected proteins. Bars, SD.

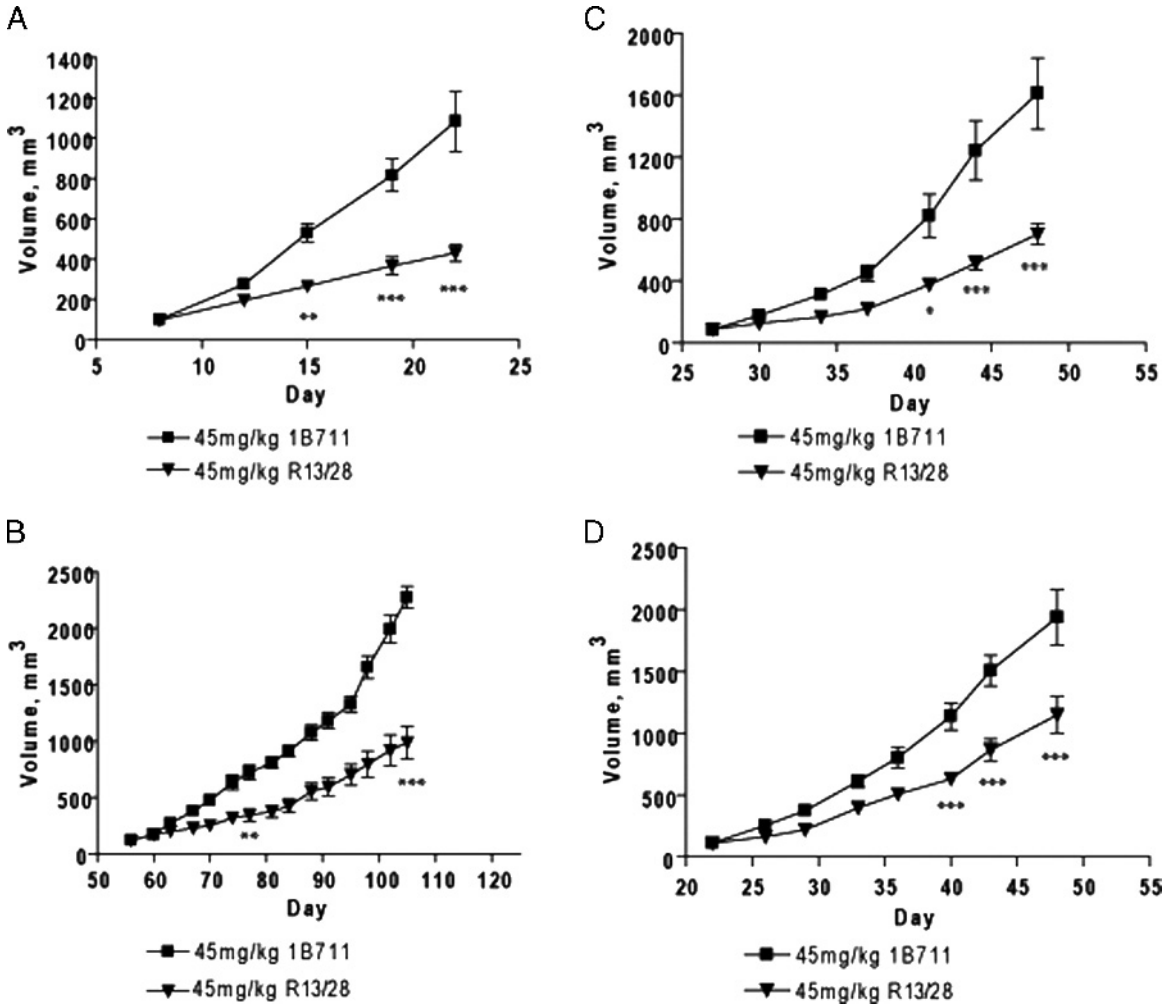

Figure 4. Combination of R13 and R28 significantly inhibits tumor growth of established human tumor xenografts *in vivo*. Established GTL-16 (A), C12 (B), C27 (C), and C28 (D) tumors (subcutaneously, $n = 10$ per group) were treated at 45 mg/kg once a week with the indicated antibodies (1B711 control antibody, black squares; R13/28, inverted triangles). R13/28 induced tumor growth inhibition (TGI) of 49% in GTL-16, 57% in C12, 56% in C27, and 41% in C28 tumors. Note that the used molar ratio of R13/R28 is 1:8, based on K_D values to rMET-ECD. Tumor volume (*x*-axis) is plotted over time (*y*-axis). Asterisks indicate significant tumor growth inhibition at day shown. Student's *t*-test, $*P < .05$, $**P < .01$, $***P < .001$. Symbols indicate mean; bars, SEM.

anti-HER2 antibody trastuzumab, which leads not only to a decrease in proangiogenic factors but also to a dramatic increase in thrombospondin, a negative regulator of angiogenesis [32].

To gain more insight in the mode of action, we analyzed the gene expression profile of R13/28–treated C27 tumors by microarray (Figure 5*B*). Interestingly, we observed that inhibition of HGF/MET pathway significantly upregulated the known tumor suppressors KLF6, CEACAM1, and BMP2 (2.3-, 2.1-, and 2.8-fold, $P < .001$) and the negative regulator of phosphatidyl-inositol-3-OH-kinase (PI3K) PIK3IP1 (2.3-fold, $P < .001$). Concurrently, SCF and SERPINE2, both enhancers of proliferation and invasiveness, were significantly suppressed (SCF, 2.4-fold; SERPINE2, 4.2-fold; $P < .001$). It has previously been shown that the tumor suppressor functions of KLF6, CEACAM1, and BMP2 are inactivated in CRC [33–36]. Moreover, SCF/KIT receptor signaling has been implicated in proliferation and invasiveness of CRC through the PI3K/AKT pathway [37]. A recent report by Zhu et al. [38] suggests that PIK3IP1 is a novel p110 interacting protein, which directly down-modulates PI3K activity. Conversely, SERPINE2 has been involved in enhancing invasive potential of pancreas cancer cells in nude mice [39]. One mode of action of R13/R28 could be the restoration of the tumor suppressor function of KLF6, CEACAM1, and BMP2, which would ultimately inhibit tumor progression. In addition, R13/R28–induced PIK3IP1 could amplify the inhibition of AKT1 phosphorylation and potentiate R13/R28–induced downregulation of SCF through abrogated PI3K activity, resulting in diminished antiapoptotic/migratory signaling.

It has previously been reported that inhibition of MET in GTL-16 strongly decreased lung metastases *in vivo* [16]. Therefore, we tested the ability of R13 and R28 to increase survival by diminishing lung metastases in an experimental metastasis model with GTL-16 cells (Figure 6). Mice were injected with GTL-16 cells stably expressing the luciferase (*luc*) gene [40] and treated weekly with R13/28 or control antibody 1B711. Treatment was stopped after 3 weeks, and the disease recurrence was measured by noninvasive imaging every week. After 70 days, five of seven mice were alive, and four of five showed strong *luc* activity in the lungs, whereas all R13/28–treated animals were alive and did not show any *luc* activity (Figure 6*A*). At day 170, only one mouse in the R13/28 treatment group died, whereas in the

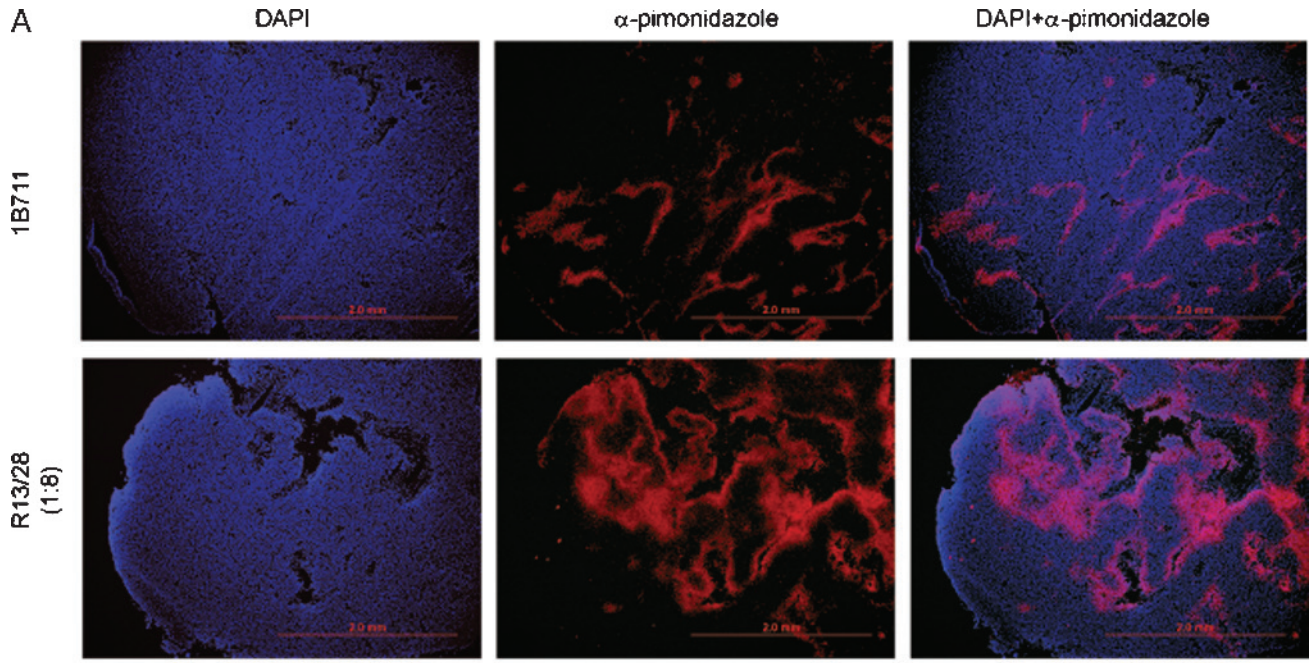

B

Gene	Fold	PVal
LOC441453	-2.25	3.10×10^{-4}
KITLG	**-2.43**	**1.46×10^{-4}**
DOK7	-2.56	6.91×10^{-5}
DCLK1	-7.05	6.79×10^{-8}
BCL11A	-3.53	3.07×10^{-5}
ACTA1	-2.08	2.32×10^{-4}
PRKACB	-2.74	1.20×10^{-4}
DHRS3	-3.58	1.42×10^{-5}
CRYAB	-3.17	2.58×10^{-4}
METTL7B	-2.05	8.53×10^{-4}
MYLPF	-3.82	1.61×10^{-4}
C11orf31	-2.80	7.30×10^{-4}
CST6	-6.56	1.88×10^{-4}
SERPINE2	**-4.20**	**5.03×10^{-4}**
PCDH10	-6.45	8.97×10^{-4}
RAB3B	3.53	8.37×10^{-4}
LMO7	2.01	2.86×10^{-4}
EDN1	2.36	9.81×10^{-4}
KLHL24	2.91	4.75×10^{-4}
LCE3D	2.86	1.01×10^{-4}
KLF6	**2.29**	**5.27×10^{-4}**
SLC12A6	2.49	6.14×10^{-4}
NOS3	2.42	3.99×10^{-4}
PIK3IP1	**2.32**	**2.69×10^{-4}**
HAS3	2.92	2.20×10^{-4}
HAPLN3	2.15	3.65×10^{-4}
SPTAN1	2.43	5.43×10^{-4}
ATG9B	3.75	3.02×10^{-5}
HLA-F	2.97	7.33×10^{-5}
KRT17	3.17	7.01×10^{-6}
AHNAK2	2.03	1.47×10^{-5}
MGC3260	2.36	5.15×10^{-4}
ARHGAP29	2.21	1.61×10^{-4}
MAP3K8	3.40	4.19×10^{-5}
TncRNA	3.74	1.32×10^{-5}
IL6R	3.03	8.30×10^{-5}
MEF2A	2.30	3.60×10^{-4}
MAST4	2.77	1.96×10^{-4}
CEACAM1	**2.14**	**3.20×10^{-4}**
TGFA	2.02	2.90×10^{-4}
ECM1	2.49	1.06×10^{-4}
BMP2	**2.76**	**2.40×10^{-4}**
DUSP5	3.86	8.29×10^{-7}
PRDM1	2.47	8.60×10^{-7}
FRMD4A	2.42	5.51×10^{-5}
LOC162993	3.66	5.02×10^{-6}
HSD11B1	48.85	8.88×10^{-16}

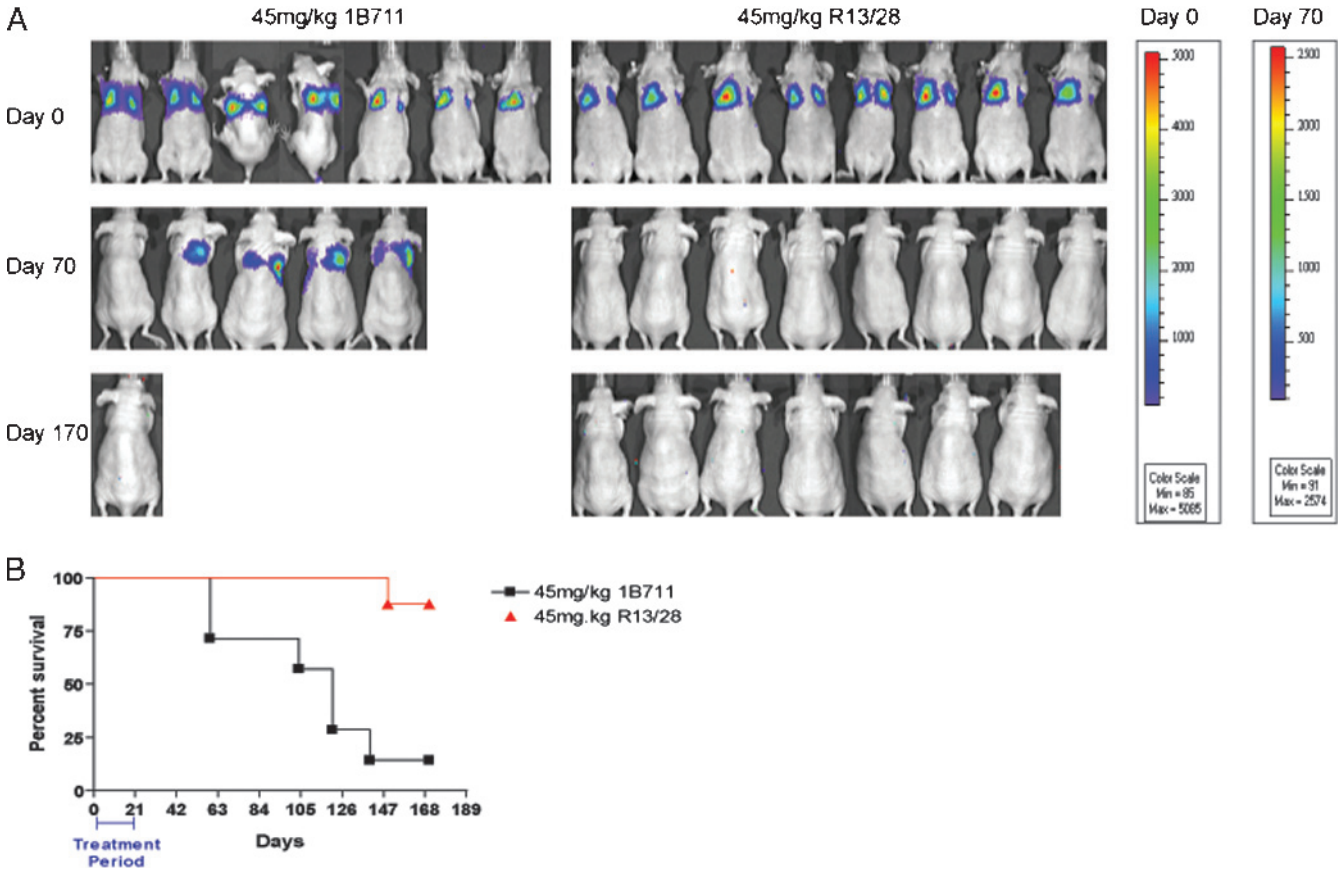

Figure 6. Combination of R13 and R28 inhibits lung colonization of GTL-16-*luc* cells and increases survival in nude (*nu/nu*) mice. After intravenous injection of (1.25×10^6 cells per mouse) GTL-16-*luc* cells, bioluminescence images were acquired after luciferin administration (150 mg/kg, intraperitoneally) (A). Tumor recurrence and survival was observed for 170 days after cell injection. Antibodies were administered once weekly from day −1 to day 21, and animals were continuously imaged every 2 weeks. To reduce stress on the animals, control antibodies 1B711 or R13/28 were injected 24 hours before mice were challenged with GTL-16 cells. Log-rank (Mantel-Cox) comparison of survival plots indicated 80% survival of R13/R28 group *versus* 0% of 1B711 group at day 170 ($P < .001$). Please note that at day 70, all mice in R13/28 group still remained tumor-free when compared with 1B711 group (B). Bar, treatment period of 21 days.

control group, six of seven mice died (Figure 6*B*). This suggests that the antibody treatment with R13/28 either inhibited the extravasation of the tumor cells and/or diminished the survival capabilities of GTL-16 in the lungs, by preventing the binding of stromal-derived HGF to MET, although murine HGF has a weaker activity in activating human MET receptor than the human counterpart. Another explanation could be that R13 or R28 acts as an inverse agonist, thereby shifting the equilibrium from the activated state toward the inactive form of MET. This shift could then lead to a decrease in proliferation and increase in the apoptotic rate of GTL-16 cells.

The discovery of fully human inhibitory antibodies against MET has so far been difficult, probably because of the structural constraints and limited accessibility to HGF binding sites. To best of our knowledge, only a "one-armed" humanized antibody has entered clinical trials [10]. We have shown that the difficult therapeutic antibody target MET can be inhibited if alternative approaches using cell-based panning are carried out. Because HGF has been shown to be an important proangiogenic factor, antiangiogenic effects in addition to antitumor/metastatic properties could therefore be expected for R13 and R28. In primary colon tumors, anti-MET antibody combination R13/28 not only sig-

Figure 5. Combination of R13 and R28 significantly upregulates hypoxia in C27 colon tumors (A). Overviews of DAPI staining and detection for hypoxic areas of representative tumor sections from 1B711- (top panel) and R13/28– (bottom panel) treated mice. Viable tumor cells are equally present in 1B711- and in R13/28–treated tumors, indicated by the relatively uniform and dense DAPI stain (top left *vs* bottom left panel). In R13/28–treated tumors, hypoxic regions (α-pimonidazole) are significantly more pronounced than in 1B711 treated tumors, which contributes to tumor growth inhibition (bottom middle *vs* top middle panel). AF594-conjugated goat antirabbit $F(Ab')_2$ was used to detect antipimonidazole antibody. Right panel is a composition of the two stains. Scale bars, 2.5 mm. Relative expression levels of selected genes significantly regulated by R13/28 treatment in the C27 xenograft tumor model (B). The expression level of each gene was normalized by *z*-score transformation across the samples in the control (CTRL) and treatment (R13/28) groups. Red and green indicate high and low expression levels, respectively. The *P* value (*P*Val) of each gene is the probability of significant regulation of the gene by R13/28 by chance using Bayesian *t*-test. Several interesting genes were highlighted by bold font and described in the text.

nificantly inhibited tumor growth by upregulating hypoxia and tumor suppressor genes but also ultimately increased survival by diminishing the number of lung metastases, presumably by interfering with the extravasation process or transition from micrometastases to macrometastases through the inhibition of survival capabilities. Recent progress in bispecific antibody design has been achieved, and we are now exploring the possibility to fuse the inhibitory properties of R13 and R28 into one therapeutic molecule [41]. In conclusion, we have shown that, in various colon cancer models, R13/28 show effective antitumor activity, which warrants further investigation and may ultimately lead to a new therapeutic molecule for colon cancer and other deadly malignancies.

References

[1] Jemal A, Siegel R, Ward E, Hao Y, Xu J, Murray T, and Thun MJ (2008). Cancer statistics, 2008. *CA Cancer J Clin* **58**, 71–96.

[2] Benson AB III (2007). Epidemiology, disease progression, and economic burden of colorectal cancer. *J Manag Care Pharm* **13**, S5–S18.

[3] Penna C and Nordlinger B (2002). Colorectal metastasis (liver and lung). *Surg Clin North Am* **82**, 1075–1090; x–xi.

[4] Boccaccio C and Comoglio PM (2006). Invasive growth: a MET-driven genetic programme for cancer and stem cells. *Nat Rev Cancer* **6**, 637–645.

[5] Birchmeier C, Birchmeier W, Gherardi E, and Vande Woude GF (2003). Met, metastasis, motility and more. *Nat Rev Mol Cell Biol* **4**, 915–925.

[6] Herynk MH, Stoeltzing O, Reinmuth N, Parikh NU, Abounader R, Laterra J, Radinsky R, Ellis LM, and Gallick GE (2003). Down-regulation of c-Met inhibits growth in the liver of human colorectal carcinoma cells. *Cancer Res* **63**, 2990–2996.

[7] Zeng ZS, Weiser MR, Kuntz E, Chen CT, Khan SA, Forslund A, Nash GM, Gimbel M, Yamaguchi Y, Culliford AT 4th, et al. (2008). c-Met gene amplification is associated with advanced stage colorectal cancer and liver metastases. *Cancer Lett* **265**, 258–269.

[8] Comoglio PM, Giordano S, and Trusolino L (2008). Drug development of MET inhibitors: targeting oncogene addiction and expedience. *Nat Rev Drug Discov* **7**, 504–516.

[9] Prat M, Crepaldi T, Pennacchietti S, Bussolino F, and Comoglio PM (1998). Agonistic monoclonal antibodies against the Met receptor dissect the biological responses to HGF. *J Cell Sci* **111** (Pt 2), 237–247.

[10] Jin H, Yang R, Zheng Z, Romero M, Ross J, Bou-Reslan H, Carano RA, Kasman I, Mai E, Young J, et al. (2008). MetMAb, the one-armed 5D5 anti–c-Met antibody, inhibits orthotopic pancreatic tumor growth and improves survival. *Cancer Res* **68**, 4360–4368.

[11] Rothe C, Urlinger S, Lohning C, Prassler J, Stark Y, Jager U, Hubner B, Bardroff M, Pradel I, Boss M, et al. (2008). The human combinatorial antibody library HuCAL GOLD combines diversification of all six CDRs according to the natural immune system with a novel display method for efficient selection of high-affinity antibodies. *J Mol Biol* **376**, 1182–1200.

[12] van der Horst EH, Degenhardt YY, Strelow A, Slavin A, Chinn L, Orf J, Rong M, Li S, See LH, Nguyen KQ, et al. (2005). Metastatic properties and genomic amplification of the tyrosine kinase gene *ACK1*. *Proc Natl Acad Sci USA* **102**, 15901–15906.

[13] Lorenzato A, Olivero M, Patane S, Rosso E, Oliaro A, Comoglio PM, and Di Renzo MF (2002). Novel somatic mutations of the *MET* oncogene in human carcinoma metastases activating cell motility and invasion. *Cancer Res* **62**, 7025–7030.

[14] Raleigh JA, Chou SC, Tables L, Suchindran S, Varia MA, and Horsman MR (1998). Relationship of hypoxia to metallothionein expression in murine tumors. *Int J Radiat Oncol Biol Phys* **42**, 727–730.

[15] Al-Hajj M, Wicha MS, Benito-Hernandez A, Morrison SJ, and Clarke MF (2003). Prospective identification of tumorigenic breast cancer cells. *Proc Natl Acad Sci USA* **100**, 3983–3988.

[16] Corso S, Migliore C, Ghiso E, De Rosa G, Comoglio PM, and Giordano S (2008). Silencing the *MET* oncogene leads to regression of experimental tumors and metastases. *Oncogene* **27**, 684–693.

[17] Zhang GJ, Chen TB, Bednar B, Connolly BM, Hargreaves R, Sur C, and Williams DL (2007). Optical imaging of tumor cells in hollow fibers: evaluation of the antitumor activities of anticancer drugs and target validation. *Neoplasia* **9**, 652–661.

[18] Baldi P and Long AD (2001). A Bayesian framework for the analysis of microarray expression data: regularized *t*-test and statistical inferences of gene changes. *Bioinformatics* **17**, 509–519.

[19] Chou TC and Talalay P (1984). Quantitative analysis of dose-effect relationships: the combined effects of multiple drugs or enzyme inhibitors. *Adv Enzyme Regul* **22**, 27–55.

[20] Schlessinger J (2000). Cell signaling by receptor tyrosine kinases. *Cell* **103**, 211–225.

[21] Fuh G (2007). Synthetic antibodies as therapeutics. *Expert Opin Biol Ther* **7**, 73–87.

[22] Rege-Cambrin G, Scaravaglio P, Carozzi F, Giordano S, Ponzetto C, Comoglio PM, and Saglio G (1992). Karyotypic analysis of gastric carcinoma cell lines carrying an amplified *c-met* oncogene. *Cancer Genet Cytogenet* **64**, 170–173.

[23] Smolen GA, Sordella R, Muir B, Mohapatra G, Barmettler A, Archibald H, Kim WJ, Okimoto RA, Bell DW, Sgroi DC, et al. (2006). Amplification of MET may identify a subset of cancers with extreme sensitivity to the selective tyrosine kinase inhibitor PHA-665752. *Proc Natl Acad Sci USA* **103**, 2316–2321.

[24] Wickramasinghe D and Kong-Beltran M (2005). Met activation and receptor dimerization in cancer: a role for the Sema domain. *Cell Cycle* **4**, 683–685.

[25] Clynes RA, Towers TL, Presta LG, and Ravetch JV (2000). Inhibitory Fc receptors modulate *in vivo* cytoxicity against tumor targets. *Nat Med* **6**, 443–446.

[26] Bussolino F, Di Renzo MF, Ziche M, Bocchietto E, Olivero M, Naldini L, Gaudino G, Tamagnone L, Coffer A, and Comoglio PM (1992). Hepatocyte growth factor is a potent angiogenic factor which stimulates endothelial cell motility and growth. *J Cell Biol* **119**, 629–641.

[27] Ma PC, Jagadeeswaran R, Jagadeesh S, Tretiakova MS, Nallasura V, Fox EA, Hansen M, Schaefer E, Naoki K, Lader A, et al. (2005). Functional expression and mutations of c-Met and its therapeutic inhibition with SU11274 and small interfering RNA in non–small cell lung cancer. *Cancer Res* **65**, 1479–1488.

[28] Christensen JG, Schreck R, Burrows J, Kuruganti P, Chan E, Le P, Chen J, Wang X, Ruslim L, Blake R, et al. (2003). A selective small molecule inhibitor of c-Met kinase inhibits c-Met–dependent phenotypes *in vitro* and exhibits cytoreductive antitumor activity *in vivo*. *Cancer Res* **63**, 7345–7355.

[29] Wang X, Le P, Liang C, Chan J, Kiewlich D, Miller T, Harris D, Sun L, Rice A, Vasile S, et al. (2003). Potent and selective inhibitors of the Met [hepatocyte growth factor/scatter factor (HGF/SF) receptor] tyrosine kinase block HGF/SF–induced tumor cell growth and invasion. *Mol Cancer Ther* **2**, 1085–1092.

[30] Zeng Z, Weiser MR, D'Alessio M, Grace A, Shia J, and Paty PB (2004). Immunoblot analysis of c-Met expression in human colorectal cancer: overexpression is associated with advanced stage cancer. *Clin Exp Metastasis* **21**, 409–417.

[31] Takeuchi H, Bilchik A, Saha S, Turner R, Wiese D, Tanaka M, Kuo C, Wang HJ, and Hoon DS (2003). c-MET expression level in primary colon cancer: a predictor of tumor invasion and lymph node metastases. *Clin Cancer Res* **9**, 1480–1488.

[32] Izumi Y, Xu L, di Tomaso E, Fukumura D, and Jain RK (2002). Tumour biology: herceptin acts as an anti-angiogenic cocktail. *Nature* **416**, 279–280.

[33] Miyaki M, Yamaguchi T, Iijima T, Funata N, and Mori T (2006). Difference in the role of loss of heterozygosity at 10p15 (KLF6 locus) in colorectal carcinogenesis between sporadic and familial adenomatous polyposis and hereditary nonpolyposis colorectal cancer patients. *Oncology* **71**, 131–135.

[34] Mukai S, Hiyama T, Tanaka S, Yoshihara M, Arihiro K, and Chayama K (2007). Involvement of Kruppel-like factor 6 (KLF6) mutation in the development of nonpolypoid colorectal carcinoma. *World J Gastroenterol* **13**, 3932–3938.

[35] Shively JE (2004). CEACAM1 and hyperplastic polyps: new links in the chain of events leading to colon cancer. *Oncogene* **23**, 9303–9305.

[36] Kotzsch A, Nickel J, Seher A, Heinecke K, van Geersdaele L, Herrmann T, Sebald W, and Mueller TD (2008). Structure analysis of bone morphogenetic protein-2 type I receptor complexes reveals a mechanism of receptor inactivation in juvenile polyposis syndrome. *J Biol Chem* **283**, 5876–5887.

[37] Yasuda A, Sawai H, Takahashi H, Ochi N, Matsuo Y, Funahashi H, Sato M, Okada Y, Takeyama H, and Manabe T (2007). Stem cell factor/c-kit receptor signaling enhances the proliferation and invasion of colorectal cancer cells through the PI3K/Akt pathway. *Dig Dis Sci* **52**, 2292–2300.

[38] Zhu Z, He X, Johnson C, Stoops J, Eaker AE, Stoffer DS, Bell A, Zarnegar R, and DeFrances MC (2007). PI3K is negatively regulated by PIK3IP1, a novel p110 interacting protein. *Biochem Biophys Res Commun* **358**, 66–72.

[39] Buchholz M, Biebl A, Neesse A, Wagner M, Iwamura T, Leder G, Adler G, and Gress TM (2003). SERPINE2 (protease nexin I) promotes extracellular matrix production and local invasion of pancreatic tumors *in vivo*. *Cancer Res* **63**, 4945–4951.

[40] Coleman JE, Huentelman MJ, Kasparov S, Metcalfe BL, Paton JF, Katovich MJ, Semple-Rowland SL, and Raizada MK (2003). Efficient large-scale production and concentration of HIV-1–based lentiviral vectors for use *in vivo*. *Physiol Genomics* **12**, 221–228.

[41] Wu C, Ying H, Grinnell C, Bryant S, Miller R, Clabbers A, Bose S, McCarthy D, Zhu RR, Santora L, et al. (2007). Simultaneous targeting of multiple disease mediators by a dual-variable-domain immunoglobulin. *Nat Biotechnol* **25**, 1290–1297.

Supplementary Data

Materials and Methods

IgG affinity measurements. FAb and/or IgG affinities were determined using a Biacore 2000 instrument (Biacore, Piscataway, NJ). Briefly, Met ECD was immobilized on a CM5 chip using standard amine-based chemistry (NHS/EDC). For each FAb and IgG, different concentrations (100-1 nM) were injected over the Met ECD surface, and kinetic data were collected over time. Data were fit using the simultaneous global fit equation to yield affinity constants (K_D) for each FAb and IgG.

Quantitative PCR. Briefly, total RNA was prepared from Oncomed's in-house tumor collection according to Qiagen's RNA isolation protocol (Valencia, CA). Total RNA was quantified, and was cDNA prepared from total RNA samples using random primers from the High-Capacity cDNA Archive Kit. Gene-specific primers and probes against human GUS-B (VIC-label) served as an endogenous control. Samples have been run in the 7900HT Fast Real-time PCR System and analyzed in quadruplicates using RQ Manager software (Applied Biosystems, Foster City, CA).

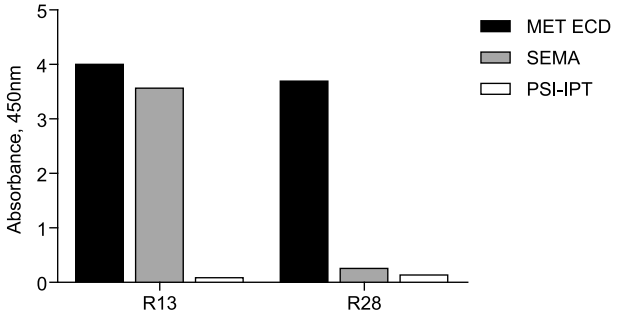

Figure W1. Epitope mapping of R13 and R28. The 384-well microtiter plates were coated with human recombinant proteins (MET-ECD, SEMA, PSI-IPT) as described previously in Materials and Methods section. Binding of R13 or R28 to individual domains of MET was determined with a standard plate reader. Please note that R28 exclusively binds to MET ECD, whereas R13 binds to the SEMA domain of MET ECD. Neither bind to PSI-IPT. Black bars, MET ECD; gray bars, SEMA; white bars, PSI-IPT.

Table W1. Summary of Inhibitory Effects of Anti-MET Antibodies.

Effect	R13 (*r*)	R28 (*r*)	R13/28 (*r*)
HGF competition IC_{50} (nM)	8.88 (0.97)	30.3 (0.99)	4.44 (0.96)
HGF competition, CI values (ED_{75})	N/A	N/A	0.52
HGF competition, CI values (ED_{90})	N/A	N/A	0.39
ADCC, IC_{50} (μM)	0.48 (0.92)	3.77 (0.99)	0.06 (0.87)
ADCC, CI values (ED_{75})	N/A	N/A	0.04
ADCC, CI values (ED_{90})	N/A	N/A	0.02
MET IC_{50} (nM), Y1230/Y1234/Y1235	N/A	N/A	49.5 (0.94)
MET IC_{50} (nM), Y1349	N/A	N/A	254 (0.99)
AKT1 IC_{50} (nM), S473	N/A	N/A	34.8 (0.94)
ERK1/2 IC_{50} (nM), T185/Y187	N/A	N/A	208 (0.94)

Note that the linear correlation coefficient *r* of the median effect plots was added next to the antibodies. Values of $r > 0.85$ were considered to indicate that measurement of the assay was accurate and conformed to mass action law.
N/A indicates not available.

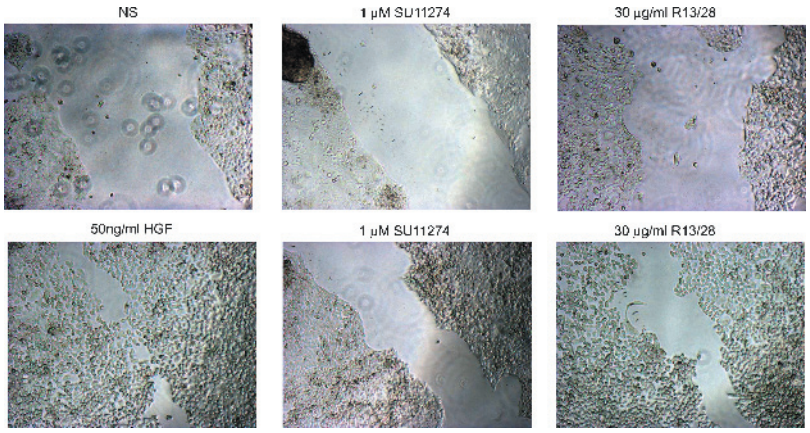

Figure W2. R13 and R28 inhibit HGF-mediated wound healing in H441 cells. H441 cells were seeded at a density of 3×10^5 cells per well in a 24-well plate. Serum-starved H441 cells pretreated with R13/28 (30 μg/ml) or SU11274 (1 μM), respectively, were used in scrape assays in the presence or absence of HGF (50 ng/ml). The scrape was monitored and photographed after 16 hours. Note that R13/28 treatment prevents HGF-induced wound closure similarly to SU11274, corroborating results in HUVECs (data not shown). The experiment was performed twice, and a representative micrograph is shown. *NS* indicates not stimulated.

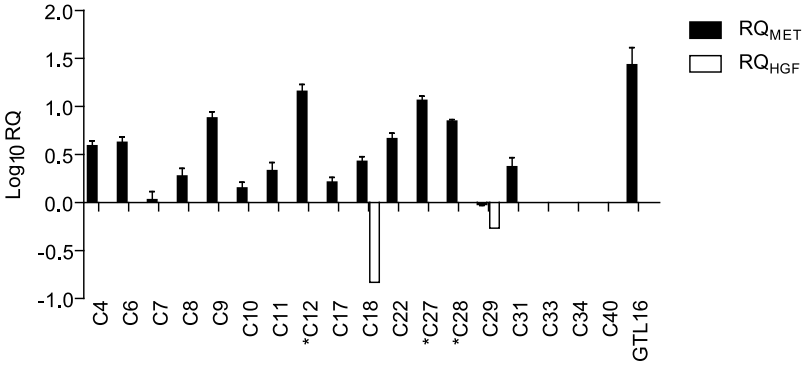

Figure W3. Expression analysis of MET and HGF in colon tumors. The analysis was performed using qualitative PCR (TaqMan) and primers and probes specific for human MET and HGF. As templates, cDNA from tumor specimen was used and analyzed in quadruplicates. Expression analysis was normalized against human GUS-B. For this analysis, the level of relative expression for MET and HGF is in comparison to the expression observed in the colon tumor specimen, OMP-C40. Please note that with the exception of C18 and C29 HGF-RNA-transcripts could not be detected, suggesting that HGF is not produced by the tumor. Asterisks indicate colon tumor models treated with R13/28. Black bars, MET; white bars, HGF; bars, SD.

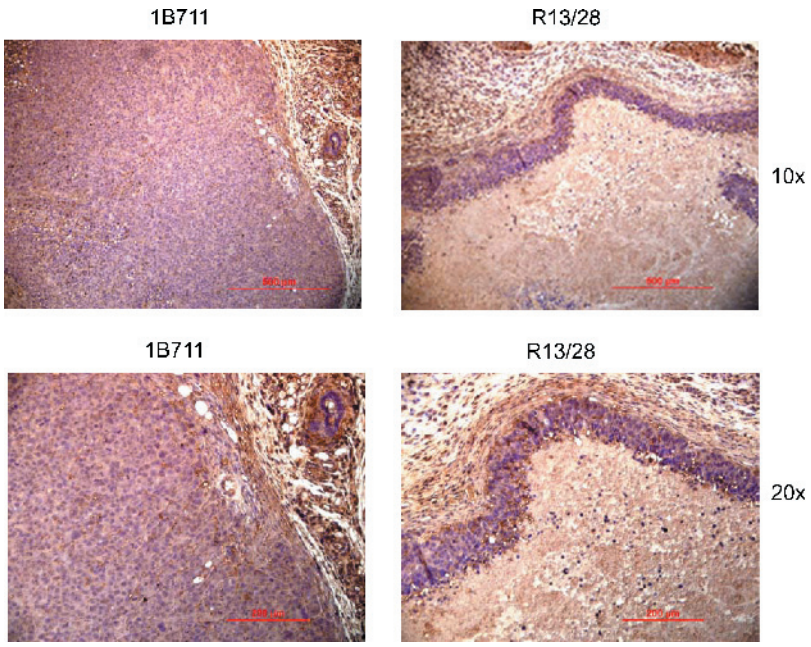

Figure W4. R13/28 significantly upregulates hypoxia in GTL-16 tumors. Overviews of hematoxylin staining and detection for hypoxic areas of representative tumor sections from 1B711 (left panel) and R13/28 (right panel) treated mice. 1B711 treatment group shows relatively uniform and dense hematoxylin stain (left *vs* right panel). However, in R13/28–treated tumors, healthy hematoxylin-stained regions are almost absent and only detectable at the rim of the tumor mass. In contrast, R13/28–treated tumors display large hypoxic regions (α-pimonidazole), especially in the center region of the tumor. Representative photographs are shown at 10- and 20-fold magnifications. Scale bars: top panel, 500 μm; bottom panel, 200 μm.